High-resolution cryo-electron microscopy of biological macromolecular structures by helical reconstruction

Koji Yonekura[1], and Saori Maki-Yonekura[2]

1. Biostructural Mechanism Laboratory, RIKEN SPring-8 Center, Harima Institute, 1-1-1 Kouto, Sayo, Hyogo 679-5148, Japan
2. Protein Crystallography Research Group, RIKEN SPring-8 Center, Harima Institute, 1-1-1 Kouto, Sayo, Hyogo 679-5148, Japan

yone@spring8.co.jp
makis@spring8.co.jp
Keywords: cryo-electron microscopy, high-resolution structure, helical reconstruction, flagellar motor, nano machine

There are many huge macromolecular complexes in living organisms. These are often hard to crystallize because of their size, complexity and heterogeneity. Cryo-electron microscopy (cryoEM) is a suitable method to analyze the structures of such biological macromolecules, because it can be applied to various forms of samples, e.g. two-dimensional crystal, helical assembly, spherical virus, dispersed particle, cell organelle and cell, although attainable resolution depends on the system. The bacterial flagellum is such an example. The flagellum is a rotary nano machine composed of ~ 30 different proteins and spins at hundreds of revolutions per second by utilizing the energy of ion flow through a membrane channel protein complex by the electrochemical potential difference across the cytoplasmic membrane. We have applied various techniques of cryoEM to analyze the flagellar structures. In 2003, we have published a ~ 4 Å resolution structure of the flagellar filament (Fig. 3) [1]. This is one of the highest resolution structures ever obtained from EM images of biological specimens without using any electron diffraction, and the very first case of visualizing twists of α-helices and some long alkyl and bulky side chains. The quality of the map allowed us to build its atomic model. To achieve this analysis, we have developed many new techniques, including accurate image alignment within individual filament images as well as between them, deconvolution of noises by solvent flattening and so on [1 - 6]. The work was reviewed as "a milestone in structural biology" in the same journal.

Bacteria swim by rotating helical flagellar filaments, which grow as long as 15 μm, but the diameter is only 120 - 250 Å. The rotary motor at the base of the filament drives the rotation of this helical propeller. For chemotaxis and thermotaxis, bacteria alternate their swimming pattern between 'run' and 'tumble', to change their swimming directions. In *E. coli and Salmonella*, the motor rotates counterclockwise (as it is viewed from outside the cell) for run, and several flagellar filaments of a left-handed supercoil form a bundle behind the cell and propel its movement. The motor reverses its rotation every few seconds, and the quick reversal produces a twisting force that transforms the left-handed supercoil into righthanded ones, by which the filament bundle falls apart rapidly. The filaments disengaged from the bundle are uncoordinated so that they generate forces that change the cell orientation and make the cell tumble. Thus, the structure of the flagellar filament and its dynamic properties play essential roles in bacterial taxis.

The flagellar filament is a long tube constructed from 11 protofilaments of a single protein, flagellin. Because of strong tendency to form the filament, flagellin is hardly crystallized. The crystal structure of a core 41 kDa fragment of flagellin (F41), which lacks about 100 residues at N- and C- termini, was solved by X-ray crystallography [7]. This

M.A. Pabst, G. Zellnig (Eds.): MC2009, Vol. 2: Life Sciences,
DOI: 10.3217/978-3-85125-062-6-154, © Verlag der TU Graz 2009

fragment cannot form any filament. To analyze the whole filament structure, we used cryoEM. We collected images of frozen-hydrated straight flagellar filaments at liquid helium temperature (~ 4K) and analyzed them by helical reconstruction with newly developed GUI tools [4]. After applying distortion correction [2] and solvent flattening [5], a density map was calculated from the data up to 4 Å resolution [1]. It shows twists of α-helices and some long alkyl and bulky side chains (Fig. 3). Then, we constructed an atomic model of full-length flagellin, and refined it by a newly developed refinement program for helical assemblies [1, 3]. The atomic model reveals that the inner domain of the filament, which is missing in F41, forms an α-helical coiled-coil structure and plays an important role in stabilizing the filament by hydrophobic interactions between flagellin subunits (Fig. 4) [1]. This result clearly demonstrates the advantage of cryoEM over X-ray crystallography, because cryoEM can be applied to physiological structures of biological macromolecules without constraints of crystal lattices (Fig. 5).

In this analysis, we have also demonstrated that a relatively small number of molecular images (~ 41,000) is sufficient to produce a high-resolution map. Excluding bad images was critical for the final map quality [3, 8]. We selected only good images giving rise to sharp and strong layer lines arranged symmetrically across the meridian (Fig. 1). It also turned out to be very important to accurately determine box-off parameters, which describe x and y- positions in a digitized image and also include the exact repeat distance and out-of-plane tilt, to extract the highest possible signals from individual images. Well-designed GUI programs were quite useful for these purposes [4]. Furthermore, three-dimensional distortion correction and solvent flattening were highly effective in improving alignment accuracy and the map quality. Three-dimensional distortions were corrected for by dividing a filament image into several segments and fitting them in the reciprocal space to a reference image. The method follows the one described by Beroukhim & Unwin [9], but is more extended to achieve better alignment and to cope with images of poor signal-to-noise ratio [2]. Solvent flattening used here has a different purpose over the standard protocol used commonly in Xray crystallography. In our method, a mask loosely enclosing the structure was first made from an initial map at lower resolution. Then, this mask was applied to three-dimensional maps calculated from individual filament images. Thereby, we can reduce noises convoluted from the solvent regions by the point-spread function of EM, and increase the image alignment accuracy [5]. See one-dimensional simulation in Fig. 2. This “individual solvent flattening” appeared to be very powerful in improving the map quality and increasing the resolution that can be obtained with a given number of images, as discussed by Yonekura & Toyoshima [5] and as shown in Fig. 4(c) of Ref. 3. Finally, the all layer-line amplitude distributions of the EM data were scaled to the structure factors calculated from an initial model, based on their radial amplitude profiles obtained by averaging the amplitudes within each resolution shell [1, 3]. It effectively increased the visibility of densities especially in the outer part of the filament and those of side chains in the inner core of the filament [1, 3].

By incorporating all these techniques into image analysis, we were able to obtain a density map at a resolution of ~ 4.0 Å with objectively meaningful structure factors as indicated by the figures of merit [1]. Based on the obtained density map, we built an atomic model of full-length flagellin in the filament structure. In X-ray crystallography, it is generally difficult to build atomic models from density maps at this resolution range because the level of phase errors is higher than that of EM. Fourier transform of EM images can give relatively reliable phase information, allowing us to build the atomic model at this resolution as shown in the structure analyses on two-dimensional crystals by using electron diffraction [10 - 13]. The model was refined using both positional and simulated annealing refinements [14], by a molecular dynamics refinement program, FEX-PLOR [1, 3], which we developed based on FX-PLOR [15] for EM image analysis of helical assemblies. In cryo-electron

M.A. Pabst, G. Zellnig (Eds.): MC2009, Vol. 2: Life Sciences,
DOI: 10.3217/978-3-85125-062-6-154, © Verlag der TU Graz 2009

micrographs, the phase data are more reliable than the amplitude data, because the amplitudes are inevitably modulated and decayed towards high resolution by the contrast transfer function (CTF) of EM while the phases are only flipped by CTF. Therefore, an amplitudeweighted phase-residual was implemented in FEX-PLOR as an effective potential energy and has been shown to work quite well [1, 3].

It is a kind of dream for us working in the field of biological and medical sciences to be able to look at the three-dimensional atomic arrangements of macromolecules and molecular assemblies without making crystals. It is not only because many of them are hard to crystallize but also because crystal packing would affect the structures, just as seen in this work, and therefore limit the functional states that we can visualize. NMR spectroscopy, which permits structure analysis in solution, still has a limitation in the molecular mass of macromolecules to be analysed; the upper limit being a few tens of kDa. CryoEM is a potentially powerful method in this regard because it can be applied to various forms of samples although attainable resolution still depends on the system as mentioned above. Our work has indicated that even single particle image analysis at near atomic resolution might not be just a dream, provided that highly accurate image alignment becomes possible. Indeed, high-resolution structures of biological specimens from EM images have recently been increasing [16 – 19].

1. K. Yonekura, S. Maki-Yonekura & K. Namba, Nature **424** (2003) p623.
2. K. Yonekura & C. Toyoshima, Ultramicroscopy **107** (2007) p1141.
3. K. Yonekura, S. Maki-Yonekura & K. Namba, Structure **13** (2005) p407.
4. K. Yonekura et al., J. Struct. Biol. **144** (2003) p184.
5. K. Yonekura & C. Toyoshima, Ultramicroscopy **84** (2000) p29.
6. K. Yonekura & C. Toyoshima, Ultramicroscopy **84** (2000) p15.
7. F.A. Samatey et al., Nature **410** (2001) p331.
8. S. Maki-Yonekura & K. Yonekura, Microsc. Microanal. **14** (2008) p362.
9. R. Beroukhim & N. Unwin, Ultramicroscopy **70** (1997) p57.
10. R. Henderson et al., J. Mol. Biol. **213** (1990) p899.
11. W. Kühlbrandt et al., Nature **367** (1994) p614.
12. K. Murata et al., Nature **407** (2000) p599.
13. E. Nogales et al., Nature **391** (1998) p199.
14. A.T. Brünger et al., Science **235** (1987) p458.
15. H. Wang & G. Stubbs, Acta Crystallogr. A **49** (1993) p504.
16. N. Unwin, J. Mol. Biol. **346** (2005) p967.
17. C. Sachse et al., J. Mol. Biol. **371** (2007) p812.
18. X. Zhang et al., Proc. Natl. Acad. Sci. USA **105** (2008) p1867.
19. W. Jiang et al., Nature, **451** (2008) p1130.
20. We are very grateful to Prof. Keiichi Namba, Osaka University and Prof. Chikashi Toyoshima, the University of Tokyo for their support.

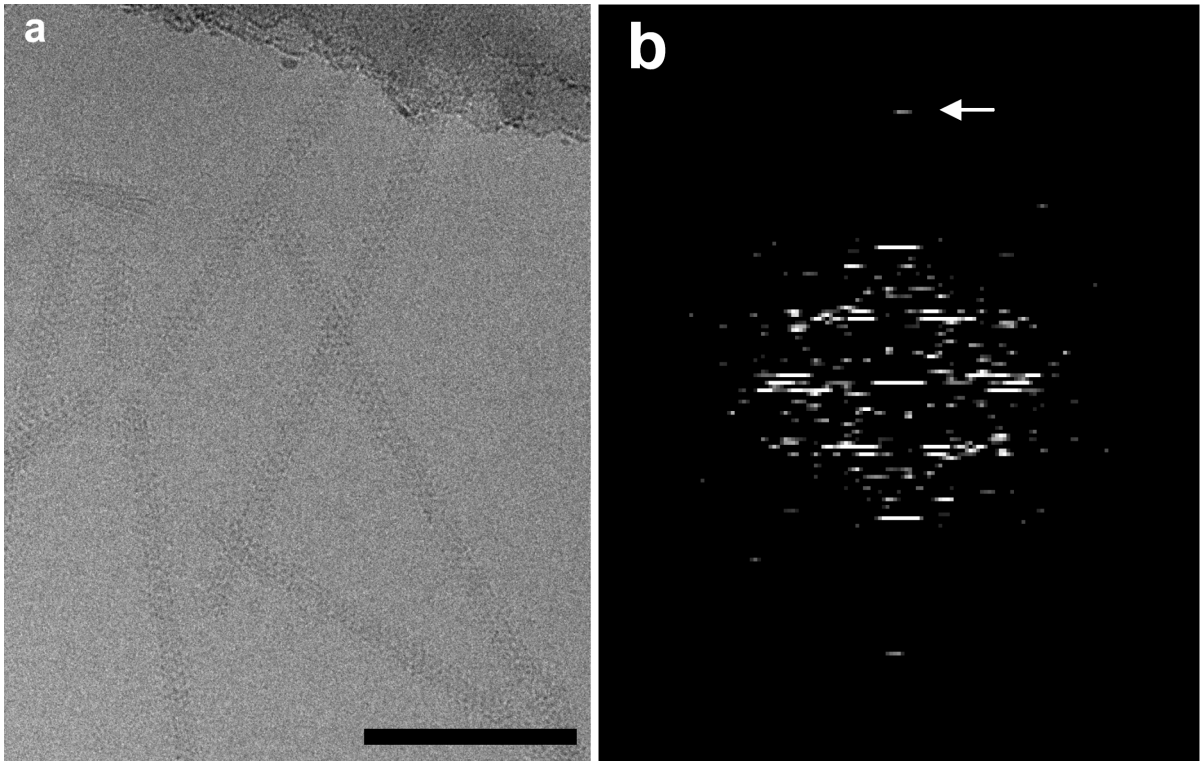

Figure 1. (a) Electron micrograph of bacterial flagellar filaments embedded in vitreous ice. Bar represents 1,000 Å. (b) Fourier transform from an image of a single flagellar filament. Arrow indicates a layer line at an axial spacing of 12.9 Å.

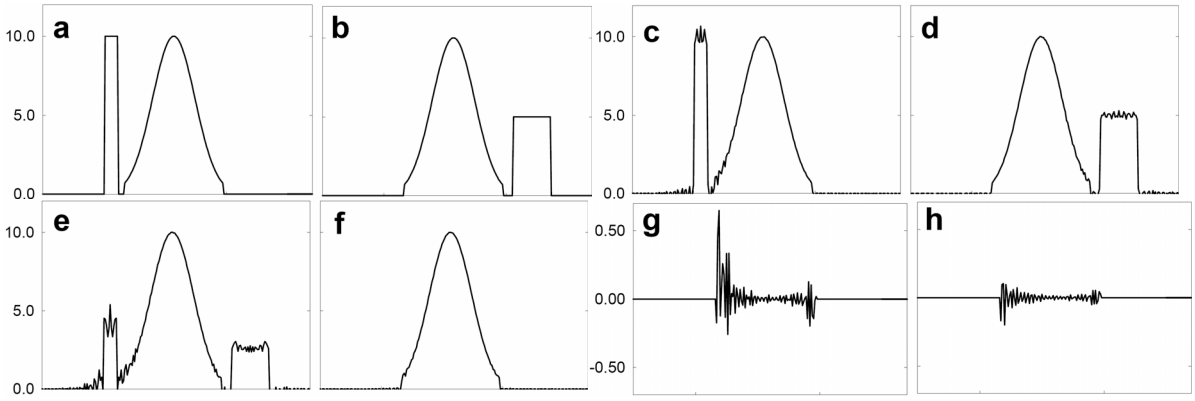

Figure 2. Dislocalisation of noise caused by CTF and its effect on the performance of solvent flattening – one-dimensional simulation. In **(a)** and **(b)**, noises (represented by rectangles) are positioned outside the signal of Gaussian profile (at the center). **(c)** The image in (a) was recorded at 7,000 Å underfocus, Fourier transformed, partially corrected for the CTF; Fourier synthesis was then carried out. **(d)** The image in (b) was recorded at 12,000 Å underfocus and treated in the same way as in (c). **(e)** CTF-weighted average (following Eq. A.1 of Ref. 5) of the images (a) and (b) recorded at, respectively, 7,000 Å and 12,000 Å underfocus and fully converted for the CTF using the averaged CTF. **(f)** The signal regions in (c) and (d) were masked off and averaged in reciprocal space with CTF weighting (following Eq. A.5 of Ref. 5). **(g)**, **(h)** Errors introduced into the signal region by these procedures (g = e – signal, *i.e.* "one-time" solvent flattening; h = f –signal, *i.e.* "individual" solvent flattening), showing the dislocation of noise. Note that the vertical scale is different in the last two frames (g, h).

M.A. Pabst, G. Zellnig (Eds.): MC2009, Vol. 2: Life Sciences,
DOI: 10.3217/978-3-85125-062-6-154, © Verlag der TU Graz 2009

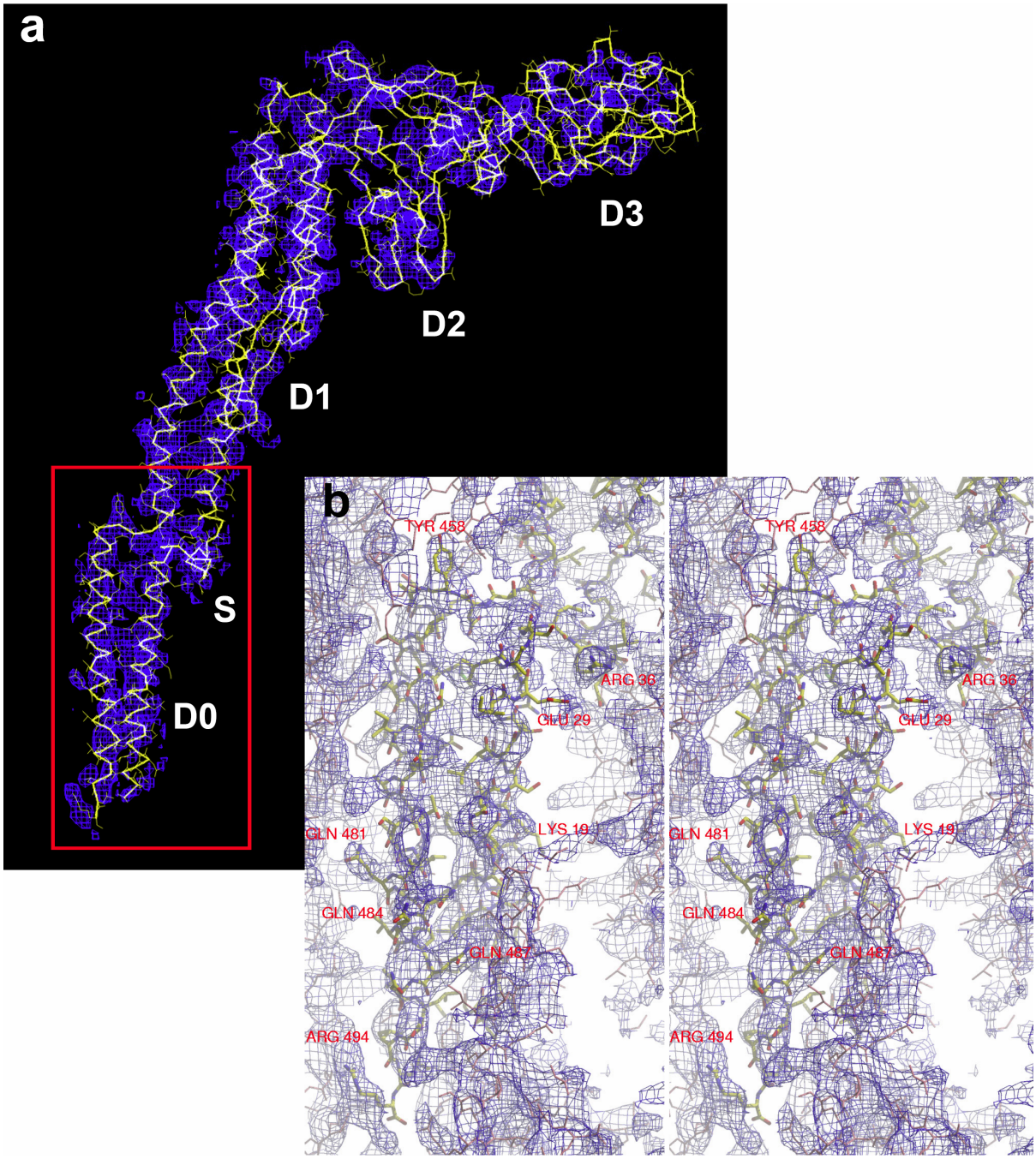

Figure 3. Density maps of the flagellar filament with the atomic model of full-length flagellin superimposed [1, 3]. **(a)** The whole molecule. Domains D0, D1, D2, D3 and the spoke region are labelled D0, D1, D2, D3 and S, respectively. **(b)** Magnified view of the terminal chains in domain D0 in stereo. The magnified area is indicated by an orange box in (**a**). The atomic model of a subunit at the center is drawn in stick and atoms are colour coded as follows: carbon, yellow; nitrogen, blue; oxygen, red. The other subunits surrounding it are drawn in thin wire and coloured pink. Contour levels of the maps are ~ 2σ.

M.A. Pabst, G. Zellnig (Eds.): MC2009, Vol. 2: Life Sciences,
DOI: 10.3217/978-3-85125-062-6-154, © Verlag der TU Graz 2009

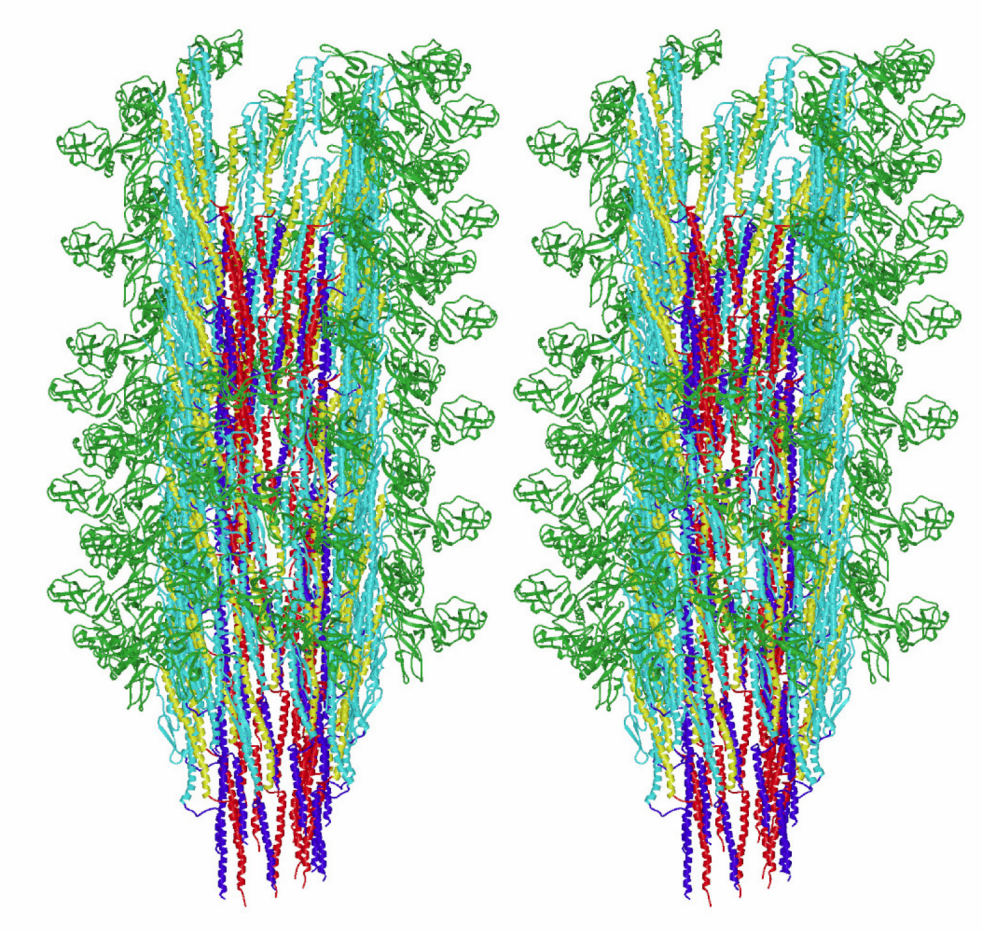

Figure 4. Ribbon diagram of the filament model in stereo view [1, 3]. Three of the 11 protofilaments are removed in the front side for the top half and in the back side for the bottom half. Top and bottom of this side view image correspond to the distal and proximal ends of the filament, respectively.

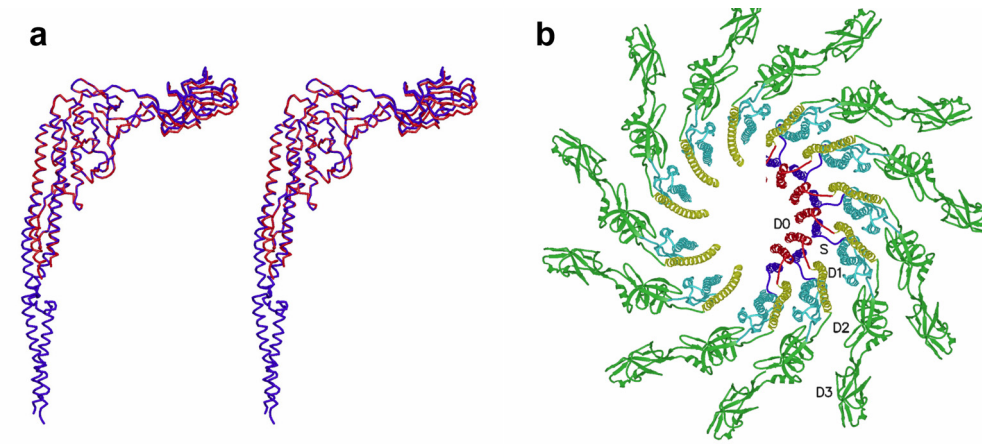

Figure 5. Comparison of the backbone of full-length flagellin in the filament with F41 in the crystal [1]. **(a)** Stereo diagram of flagellin (blue) and F41 (red). **(b)** End-on view of the filament model made of F41 (left half) and full-length flagellin (right half).

M.A. Pabst, G. Zellnig (Eds.): MC2009, Vol. 2: Life Sciences,
DOI: 10.3217/978-3-85125-062-6-154, © Verlag der TU Graz 2009